DOI 10.3217/978-3-99161-099-1-006
CC BY 4.0, https://creativecommons.org/licenses/by/4.0/deed.de
Diese CC-Lizenz gilt nicht für Materialien von Dritten und anderweitig gekennzeichnete Inhalte.

# 6

# Energy-Maximizing Regenerative Braking for Battery-Electric Regional Rail Under SOC Limits

*Amir Torkiharchegani, Lund (Sweden); François Cabillon, Piossasco (Italy); Rickard Persson, Stockholm (Sweden); Thomas Müller, Stuttgart (Germany); Christoffer Ahrling and Mats Alaküla, Lund (Sweden)*

This paper presents a route-aware regenerative-braking management approach that coordinates electrodynamic braking with speed-dependent motor limits, state-of-charge (SOC)-dependent battery charge acceptance, auxiliary-load use, and low-speed friction requirements. The train-level control system predicts speed-change and station-stop events from route profile, gradients, speed limits, auxiliary demand, and battery SOC, then adjusts braking onset and duration to keep planned service braking predominantly electrodynamic. A 120 km/h reference stop gives about 4.6 kWh initial kinetic energy and about 3.3 kWh electrodynamic reference recovery when only the electric-machine efficiency profile is considered. In the TSI 80 km/h, 21‰ (per mille), 46 km downhill case, 410 kWh and 210 kWh batteries at 50% initial SOC absorb regenerative power with negligible charge rejection. Finally, the Borlänge-Malung route is used to evaluate repeated speed-change and station-stop events, showing that battery size affects SOC headroom and regenerative capture.

## 6.1 Introduction

Battery-electric regional rail vehicles are being developed for non-electrified and partially electrified routes where full overhead-line electrification may be difficult to justify. Recent studies have therefore addressed energy use, drivetrain design, battery sizing, cost, emissions, and route-based simulation for small regional rail vehicles [1,2]. In this context,

regenerative braking is important because the onboard battery is both traction energy source and braking-energy sink.

Regenerative braking has been widely studied in electric rail systems. Regenerative braking energy can be reused by other trains, stored onboard or wayside, recovered through reversible substations, or dissipated when no suitable sink is available [3-4]. Battery-electric regional vehicles introduce a specific constraint: recovered energy must be accepted by the onboard battery at the instant of braking. Thus, producible electrodynamic braking energy and actually stored energy are not the same quantity.

Two limits dominate this gap. First, the traction system is speed dependent. At high speed, the motor-inverter system is power-limited; at very low speed, regenerative power becomes very small because motor speed is low. Electrodynamic braking can therefore be the primary service-braking actuator over the useful speed range, provided that route prediction and battery headroom are managed, while mechanical friction braking remains necessary for low-speed stopping, holding, parking, degraded operation, and emergency-related functions. Second, battery charge acceptance depends on SOC, charge current or C-rate, voltage, and temperature, while the charging protocol also affects ageing [5,6].

Brake blending is therefore linked to both braking control and energy management. As used here, local brake blending denotes the allocation of a train-level brake demand between electrodynamic and mechanical friction braking, while route prediction and braking-timing adaptation are handled at train-control level. The LOC&PAS TSI identifies dynamic braking as linked to the traction system [7] while EN 15595 addresses wheel-slide protection acceptance and implementation [8]. This work does not replace safety functions. Adhesion and WSP are treated as supervisory layers; the focus is service-braking allocation that maximizes stored regenerative energy.

Gradient, speed profile, auxiliary demand, and braking timing strongly affect regenerative capture. Train-control studies show that speed profile, braking onset, coasting, and timetable margins influence energy use [9]. Related regional-train work has addressed speed adjustment under route and seasonal conditions [10], and energy transfer between battery-powered trains or infrastructure [11].

Here, a train-level driving and braking management function estimates braking energy and allowable pre-event SOC for each upcoming event. If route and timetable margins allow, it requests earlier braking or a lower approach speed to reduce peak regenerative power, while the local brake-blending function allocates the resulting brake demand between electrodynamic and mechanical friction braking. The method is evaluated using a 120 km/h reference stop, the TSI long downhill case, and the Borlänge-Malung route.

## 6.2 Braking constraints and control concept

For a braking demand generated at train level, the local brake-blending function divides the requested braking power between electrodynamic and mechanical friction braking:

$$P_{brake,req} = P_{ED} + P_{fric} \quad (1)$$

The admissible electrodynamic braking power is limited by braking demand, motor-inverter capability, and available absorption capacity:

$$P_{ED,adm} = \min\left(P_{\mathrm{brake},req}, P_{ED,\max\,(\mathrm{v})}, P_{batt,\max\,(\mathrm{SOC})} + P_{sink,max}\right) \quad (2)$$

Here $P_{ED,max(v)}$ is the speed-dependent motor-inverter braking limit, $P_{bat,max(SOC)}$ is the admissible battery charge power, and $P_{sink,max}$ represents auxiliary loads or other available sinks. The friction-brake demand is

$$P_{fric} = max, (0, P_{brake,req} - P_{ED,adm}) \quad (3)$$

In implementation, the local brake control uses the achieved electrodynamic (ED) braking effort to command the remaining mechanical friction-brake effort. This allocation distinguishes two causes of friction use. Motor-limited shortfall occurs when the traction system cannot provide the requested braking power. At train-control level, it can often be reduced by earlier braking, longer braking duration, or lower approach speed. Charge-limited shortfall occurs when the motor could produce ED braking but the battery and other sinks cannot absorb it; it requires SOC headroom, auxiliary or external absorption, energy transfer, or fallback friction/dissipation.

For a predicted event k, the maximum allowable pre-event SOC is approximated by

$$SOC_{max,k} = SOC_{upper} - \left(\frac{E_{reg,pred,k}}{E_{bat,nom}} \times 100\right) \quad (4)$$

SOC values in Eq. (4) are expressed in percent. $E_{reg,pred,k}$ is the predicted regenerative energy of the braking event *k* and $E_{bat,nom}$ is nominal battery energy. This shows why smaller batteries require lower SOC before the same event: the same recovered energy causes a larger SOC increase and higher charge-rate demand. The auxiliary load is included as an onboard sink. It does not create additional recovered energy, but it can reduce battery charge-power peaks and delay curtailment. The braking hierarchy is ED-first for planned service braking; friction for low-speed stopping, holding, parking, degraded operation, safety requirements, and unavoidable residual demand; and magnetic track braking, where fitted, only as an emergency function.

## 6.3 Simulation model and case definitions

The simulation represents a 30 t battery-electric regional rail vehicle following route profiles with distance, speed reference, gradient, stops, and speed restrictions. Running resistance is modelled by the Davis equation

$$F_{res}(v) = a + b \times v + c \times (v)^2 \quad (5)$$

where *v* is speed in km/h. The simulations use a=400 N, b=2 N/(km/h), c=0.2 N/(km/h)$^2$, maximum electrical traction/regenerative power 390 kW, and a low-speed friction transition around 5 km/h. Using the 30 t vehicle, Davis running resistance, 390 kW maximum traction power, and 25 kN maximum tractive effort, the calculated acceleration time from standstill to 120 km/h on level track is approximately 59.4 s.

The battery is represented by the SOC-dependent LFP charge-power envelope used in [1] including the corresponding charge-current/C-rate limitation. Detailed electrochemical, thermal, and ageing behavior is outside the present scope. The model records stored regenerative energy, friction energy, curtailed energy, peak regenerative power, braking time, braking distance, and SOC change for each event. Three case groups are used.

1. A stop from 120 km/h provides a reference for kinetic energy and ED recovery, and is repeated under several constant gradients.
2. A TSI long-downhill case evaluates 80 km/h speed regulation on 21‰ downhill slope over 46 km.
3. The Borlänge-Malung route in Sweden evaluates repeated speed-change and station-stop events.

Route-level performance is measured by

$$R_{cap} = \frac{E_{reg,stored,total}}{E_{reg,prod,max,total}} \quad (6)$$

Here, $R_{cap}$ is the route-level regenerative capture ratio, $E_{reg,stored,total}$ is the total regenerative energy stored in the battery over the route, and $E_{reg,prod,max,total}$ is the maximum producible regenerative energy over the same route before battery charge-acceptance or SOC limits are applied. When reported as a percentage, $R_{cap}$ is multiplied by 100.

## 6.4 Results and discussion

The stop from 120 km/h on level track defines the braking-energy scale. For the 30 t vehicle, the initial kinetic energy is about 4.6 kWh. With the ED-only strategy and the electric-machine efficiency profile, the recovered reference energy is about 3.3 kWh, or

about 70%. This value is an electrodynamic reference based on the electric-machine efficiency only, not the final battery-stored energy after converter, mechanical, battery, auxiliary, or low-speed friction-related losses. Figure 1 shows that downhill gradients increase the energy to be absorbed, while uphill gradients reduce it. This recovery potential is useful only if the drivetrain limits, battery acceptance, and SOC headroom allow regenerative energy capture. The same figure motivates braking-time extension: in ATO or driver-advisory operation, earlier braking or lower approach speed can be requested when route and timetable margins allow, keeping regenerative power within limits.

The TSI long-gradient case evaluates 80 km/h speed control on a 21‰ descent over 46 km, corresponding to about 966 m altitude decrease and about 79 kWh gravitational energy before losses. Figure 2 compares 410 kWh and 210 kWh batteries at 50% initial SOC. The plotted quantities are powers in kW, except for SOC, which is shown in %. The horizontal axis is time in seconds. Non-charge power denotes regenerative power that cannot be absorbed by the battery or onboard sinks, whereas $P_{friction}$ denotes the mechanical friction-brake power required to meet the total braking demand. $P_{traction}$ denotes traction-system power, where negative values correspond to regenerative braking. SOC is the battery state of charge. In both cases, the non-charge signal remains close to zero during the main downhill section, showing that regenerative power is absorbed by the battery and onboard loads. The 410 kWh case uses friction mainly at the low-speed transition. In the 210 kWh case, a larger transient friction contribution appears under the imposed braking-time profile, but this does not mean ED braking is fundamentally insufficient. With extended braking time or distance, the same speed reduction could be achieved with lower peak regenerative power, thereby reducing the friction share. The captured energy is almost unaffected because the battery still accepts nearly all regenerative energy during steady downhill operation, with the 410 kWh and 210 kWh cases differing by only about 0.01-0.02 kWh/km in the net values reported below. The net battery-energy change over the 46 km downhill section, divided by distance, is similar when SOC headroom is sufficient. Negative

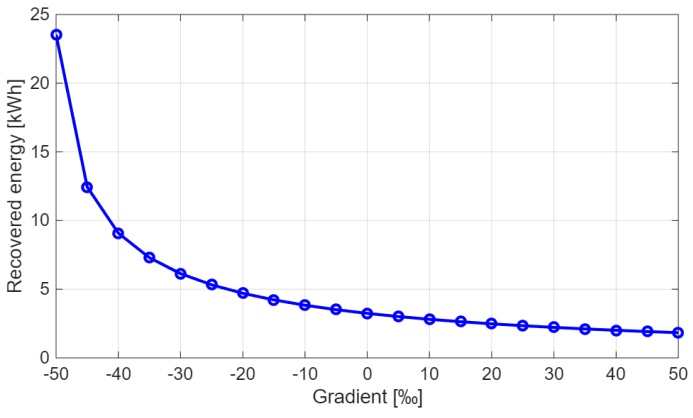
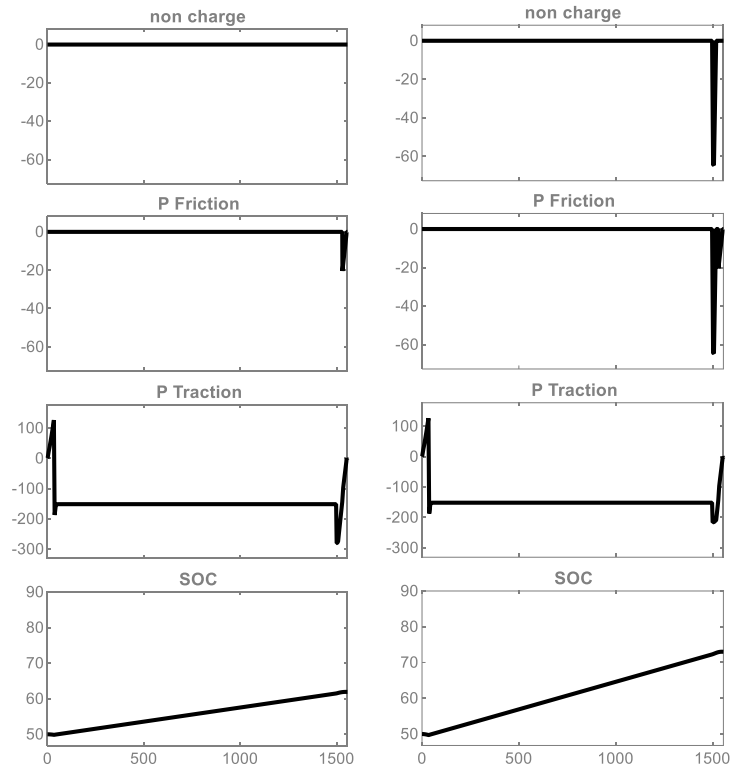



Figure 1: Reference ED braking from 120 km/h and gradient sensitivity from -50‰ to +50‰.




(a) (b)

Figure 2: TSI long-gradient speed control at 80 km/h on 21‰ descent over 46 km: (a) 410 kWh battery and 50% initial SOC; (b) 210 kWh battery and 50% initial SOC. Power traces are shown in kW, SOC in %, and time in s.

values indicate a net increase in battery energy during the descent. For the 410 kWh battery, this value is about -1.0 kWh/km with no auxiliary electrical load and about -0.8 kWh/km with a 15 kW onboard auxiliary electrical load, representing continuous non-traction demand such as HVAC, cooling, control systems, and other hotel loads. The corresponding values for the 210 kWh battery are nearly identical, about -1.0 kWh/km and about -0.8 kWh/km, because both batteries have sufficient charge-power acceptance in this case. The auxiliary demand reduces the net stored battery energy, but at high SOC it can reduce battery charge-power peaks and delay curtailment.

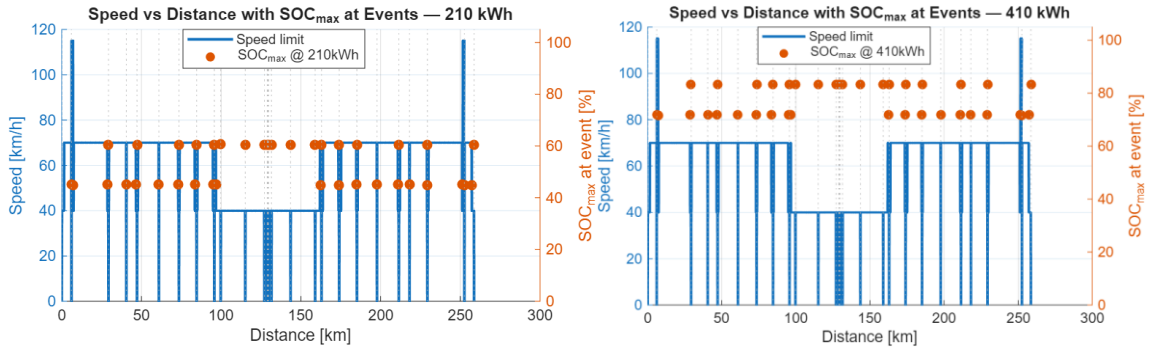
The Borlänge-Malung route case shows why event prediction is needed. Each speed-change or station-stop has different speed, gradient, braking time, distance, peak power, and recovered energy. Table 1 gives representative events. For example, the 115 to 40 km/h event near 7.1 km recovers about 2.7 kWh over 31 s and 695 m, while the 115 to 0 km/h event near 252.5 km recovers about 3.3 kWh over 47.5 s and 826 m. Figure 3 shows that the smaller battery requires lower permissible pre-event SOC, since the same recovered energy causes a larger SOC increase and higher charge-rate demand. This means that battery size affects not only nominal energy capacity, but also the usable SOC operating window available for regenerative braking. For smaller batteries, route feasibility therefore depends on the complete traction-energy balance, charging opportunities along the route,

| Position [m] | Speed from [km/h] | Speed to [km/h] | Gradient [%] | Recovered energy [kWh] | Braking Time [s] | Braking distance [m] | Peak rege-nerative power [kW] |
|---|---|---|---|---|---|---|---|
| 6,100 | 70 | 0 | 0.39 | 1.2 | 23 | 217 | 325 |
| 7,100 | 115 | 40 | 0.09 | 2.7 | 31 | 695 | 328 |
| 28,700 | 70 | 40 | 0.09 | 0.8 | 10 | 152 | 325 |
| 29,300 | 40 | 0 | 0.09 | 0.4 | 13 | 69 | 226 |
| … | … | … | … | … | … | … | … |
| 251,231 | 70 | 40 | -0.09 | 0.8 | 10.5 | 159 | 325 |
| 252,531 | 115 | 0 | -0.39 | 3.3 | 47.5 | 826 | 329 |
| 257,231 | 70 | 40 | -0.39 | 0.8 | 11 | 166 | 325 |
| 258,631 | 40 | 0 | -0.39 | 0.4 | 14 | 73 | 227 |

Table 1: Representative simulated route-level braking events

and maintaining sufficient predicted SOC headroom before braking events. The event table is therefore used to illustrate the range of braking conditions, while the overall regenerative capture is quantified at route level using Eq. (6).

In the analysed route output, the simulated maximum producible regenerative energy is approximately 29 kWh. The 410 kWh case stores about 28 kWh, corresponding to 96% capture, while the 120 kWh sensitivity case stores 24 kWh, corresponding to about 83%. The results support a control-first hierarchy: preserve SOC headroom, adapt speed profile, extend braking time where possible, use auxiliary or external sinks, and apply friction only for low-speed stopping, unavoidable residual demand, degraded operation, or safety-related functions.




(a) (b)

Figure 3 Predicted maximum pre-event SOC at braking events for (a) 210 kWh and (b) 410 kWh batteries on the Borlänge-Malung route.

## 6.5 Summary

This paper demonstrates the need for route-aware regenerative-braking management in battery-electric regional rail vehicles, coordinated across train-level control, signalling, and local brake blending. With sufficient SOC headroom, electrodynamic braking can remain

the dominant service-braking mode, while high SOC or restrictive charge-power limits require predictive measures including SOC-headroom planning, speed-profile adjustment, auxiliary-load scheduling, or longer braking. Because braking events differ in energy content and pre-event SOC requirement, smaller batteries require lower SOC and are more prone to regenerative curtailment. Mechanical friction braking remains necessary mainly for low-speed stopping and fallback conditions.

## Acknowledgements

Funded by the European Union. Views and opinions expressed are, however, those of the author(s) only and do not necessarily reflect those of the European Union or the Europe's Rail Joint Undertaking. Neither the European Union nor the granting authority can be held responsible for them. The project Flagship Project 6 (FP6) FUTURE is supported by the Europe's Rail Joint Undertaking and its members.

## Literature

[1] A. Torkiharchegani and M. Alaküla, "Enhancing Regional Rail Efficiency and Reducing Emissions with Dual Electric Traction Machine Drivetrain," IEEE Transactions on Vehicular Technology, 2025, doi: 10.1109/TVT.2025.3637539.

[2] C. Ahrling et al., "Assessing energy use, cost, and emissions of small regional rail vehicles: methodology and case study on a German track," in WCX SAE World Congress Experience 370157, 2026.

[3] A. González-Gil, R. Palacin, and P. Batty, "Sustainable urban rail systems: Strategies and technologies for optimal management of regenerative braking energy," Energy conversion and management, vol. 75, pp. 374-388, 2013.

[4] M. Khodaparastan, A. A. Mohamed, and W. Brandauer, "Recuperation of regenerative braking energy in electric rail transit systems," IEEE Transactions on Intelligent Transportation Systems, vol. 20, no. 8, pp. 2831-2847, 2019.

[5] A. Tomaszewska et al., "Lithium-ion battery fast charging: A review," etransportation, vol. 1, p. 100011, 2019.

[6] S. S. Zhang, "The effect of the charging protocol on the cycle life of a Li-ion battery," Journal of power sources, vol. 161, no. 2, pp. 1385-1391, 2006.

[7] (2014). Commission Regulation (EU) No 1302/2014 of 18 November 2014 concerning a technical specification for interoperability relating to the 'rolling stock — locomotives and passenger rolling stock' subsystem of the rail system in the European Union.

[8] EN 15595:2018+A1:2023, Railway applications — Braking — Wheel slide protection, E. C. f. Standardization, Brussels, Belgium, 2023.

[9] G. M. Scheepmaker, R. M. Goverde, and L. G. Kroon, "Review of energy-efficient train control and timetabling," European Journal of Operational Research, vol. 257, no. 2, pp. 355-376, 2017.

[10] A. Torkiharchegani et al., "Optimizing energy consumption of regional trains through speed adjustment: a seasonal and regional perspective," in rev2025–2nd Resource Efficient Vehicles Conference, 2025, p. 213, doi: 10.25364/978-3-903374-48-5_22.

[11] A. Torkiharchegani et al., "Enhancing energy efficiency and environmental sustainability through regional battery-powered train energy transfer systems," in rev2025–2nd Resource Efficient Vehicles Conference, 2025, p. 307, doi: 10.25364/978-3-903374-48-5_31.